IEEE Photonics Journal
An IEEE Photonics Society Publication

Open Access

Refractive Index and Temperature Sensing Based on an Optoelectronic Oscillator Incorporating a Fabry–Perot Fiber Bragg Grating

Volume 10, Number 1, February 2018

Yuguang Yang
Muguang Wang
Ya Shen
Yu Tang
Jing Zhang
Yue Wu
Shiying Xiao
Jingxuan Liu
Buzheng Wei
Qi Ding
Shuisheng Jian

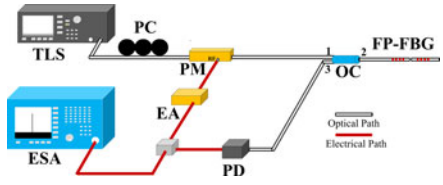

DOI: 10.1109/JPHOT.2017.2778224
1943-0655

IEEE photonics SOCIETY

IEEE

Refractive Index and Temperature Sensing Based on an Optoelectronic Oscillator Incorporating a Fabry–Perot Fiber Bragg Grating

Yuguang Yang, Muguang Wang, Ya Shen, Yu Tang, Jing Zhang, Yue Wu, Shiying Xiao, Jingxuan Liu, Buzheng Wei, Qi Ding, and Shuisheng Jian

Key Laboratory of All Optical Network and Advanced Telecommunication Network, Ministry of Education, Institute of Lightwave Technology, Beijing Jiaotong University, Beijing 100044, China

DOI:10.1109/JPHOT.2017.2778224

Manuscript received October 15, 2017; revised November 14, 2017; accepted November 25, 2017. Date of publication November 28, 2017; date of current version January 3, 2018. This work was supported by the National Natural Science Foundation of China under Grants 61475015 and 61775015.
Corresponding author: M. Wang (e-mail: mgwang@bjtu.edu.cn).

Abstract: An ultrafast high-sensitivity refractive index (RI) and temperature-sensing system based on an optoelectronic oscillator (OEO) is proposed and demonstrated in this paper. A Fabry–Perot fiber Bragg grating (FP-FBG), which combines a gap with two FBGs in a silica V-shaped slot and characterizes a narrow notch in the reflection spectrum, is incorporated in the OEO to implement a microwave photonic filter and perform oscillating frequency selection. A microwave signal is generated by the OEO, whose oscillating frequency is determined by the center frequency of the FP-FBG notch, which varies with the surrounding environments. The RI or the temperature change can be accordingly measured by monitoring the frequency shift of the microwave signal using an electrical spectrum analyzer or a digital signal processor. An experiment is performed to verify the proposal. An RI sensitivity of 413.8 MHz/0.001RIU and a temperature sensitivity of 2516 MHz/°C are successively demonstrated.

Index Terms: Fiber optics sensors, microwave photonics, fiber Bragg grating, Fabry-Perot.

1. Introduction

Refractive index (RI) sensing is needed in various biochemistry fields, including environmental monitoring, medicinal development, bio-sensing and so on. It has been proved that optical fiber sensor possesses great potential for practical application in RI sensing because of its intrinsic advantages, such as low cost, compact structure and immunity to electromagnetic interference, etc. To monitor the RI, numerous configurations of the optical fiber sensors have been demonstrated in recent years, including Fabry-Perot interferometers [1], surface plasmon resonance sensors [2], microfiber sensors [3], tapered fiber sensors [4] and so on. However, the schemes mentioned above are generally implemented by monitoring optical power or wavelength shift using an optical spectrum analyzer (OSA), which has a relatively poor interrogation speed and resolution due to limited scanning rate and wavelength resolution of the OSA.

In the past few years, various sensing approaches based on an optoelectronic oscillator (OEO) have been reported [5]–[9]. By mapping the measurand to the frequency of microwave signal generated by the OEO, a scheme of the frequency interrogation of the microwave signal using an electrical spectrum analyzer (ESA) can drastically improve the interrogation speed and resolution of the sensor system. Meanwhile, a digital signal processor (DSP) also seems to have a great potential in real engineering applications. For example, an OEO based on a phase-shifted fiber Bragg grating (PS-FBG) was first proposed by Li *et al.* [10] followed by a thermal-insensitive interrogation of a strain sensor with a resolution of 0.83 $\mu\varepsilon$ based on a modified dual-frequency OEO was demonstrated [6]. In [7], a transverse load sensor based on a dual-wavelength fiber ring laser incorporating an injection-coupled OEO was proposed with a resolution of 0.00441 N/m. In [8], a dual-frequency OEO by utilizing a polarization-maintaining fiber Bragg grating (PM-FBG) Fabry-Perot filter was proposed by us for high-sensitivity and high-speed axial strain and temperature simultaneous sensing. The general principle of the above OEO schemes for optical sensing is translating the wavelength change in the optical domain induced by measurands to the frequency change in the microwave domain. Then a high-resolution and high-speed interrogation for the target parameter measurement is obtained with high signal-to-noise ratio (SNR), owing to an inherent ultralow phase noise of the OEO-generated microwave signal. Lam Duy Nguyen *et al.* also presented for the first time a preliminary experiment for RI measurements using an OEO [9]. In this approach, a cell of liquid with unknown RI was inserted as a part free space propagation optical path of the global OEO loop. Thus a change of liquid RI would lead to a variation of the equivalent fiber loop length as well as the whole loop delay τ_g, which determines the oscillation microwave frequency and free spectral range (FSR) of the OEO by $f_m = k/\tau_g = k \cdot FSR(k = 1, 2 \cdots)$. By monitoring the change of microwave frequency or FSR of OEO, the RI of liquid was measured. However, due to the small FSR of the OEO loop with a fiber loop length of 1.5 km, the sensing range of RI is extremely limited in this architecture. In addition, the long fiber path of the loop is susceptible to surrounding environmental influences such as temperature and mechanical vibration, which would also be converted to microwave frequency change and may degrade measuring accuracy of the sensing system.

In this paper, we propose and demonstrate an approach to perform a high speed and high sensitivity frequency interrogation of the RI and temperature sensor, which is implemented by an OEO incorporating a special Fabry-Perot fiber Bragg grating (FP-FBG). The FP-FBG works as a sensing head as well as a microwave frequency selective element in joint use with a phase modulator (PM) and laser source. The FP-FBG, which characterizes a narrow notch in the refection spectrum, is fabricated by axially aligning two identical FBGs in a silica V-shape slot and the cross sections of two FBGs are separated by a gap. When the surrounding temperature of FP-FBG or the RI of liquid filled in the gap changes, the center wavelength of the notch of the FP-FBG varies, which is then converted to a microwave frequency shift by the OEO. The relationship between the frequency of the microwave signal and the RI or temperature is investigated both theoretically and experimentally.

2. Principle

Fig. 1 shows the schematic of the proposed FP-FBG based OEO for RI and temperature sensing system. An optical carrier from a tunable laser source (TLS) is sent to a PM via a polarization controller (PC). The PC is used to align the polarization direction of the optical carrier to the principal axis of the PM. Through the PM, a phase-modulated signal is generated and sent to an FP-FBG. A reflected signal by the FP-FBG is detected by a photodetector (PD). The detected microwave signal is sent to an electrical amplifier (EA) and fed back to the PM to close the OEO loop. Meanwhile, the spectrum of the microwave signal, which is generated by the OEO at the output of the PD, is monitored by an electrical spectrum analyzer (ESA).

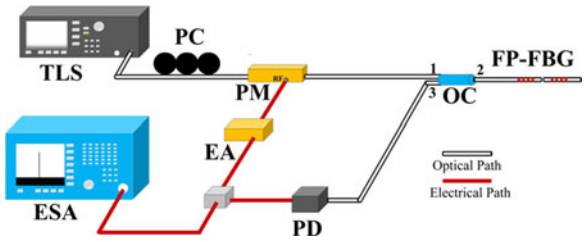

Fig. 1. Schematic of the proposed RI and temperature sensor.

Mathematically, the electrical field of the phase-modulated signal via the PM is given by

$$\begin{aligned} E_{PM}(t) &= E_0 \exp\left\{ j\left[\omega_c t + \pi \frac{V_e}{V_\pi} \cos(\omega_M t) \right] \right\} \\ &\approx E_0 \left\{ J_0(\beta) e^{j\omega_c t} + J_1(\beta) e^{j[(\omega_c+\omega_M)t+\frac{\pi}{2}]} \right. \\ &\quad \left. - J_1(\beta) e^{j[(\omega_c-\omega_M)t-\frac{\pi}{2}]} \right\} \end{aligned} \tag{1}$$

where ω_c and ω_M are the angular frequencies of the optical carrier and the microwave signal respectively, V_e is the voltage applied to the PM and V_π is the half-wave voltage of the PM. According to Eq. (1), when the phase-modulated signal is injected into the PD to perform optical-to-electrical conversion, the beating between the optical carrier and the $+1$st order sideband will be cancelled completely by another beating between the optical carrier and the -1st order sideband, due to the π phase difference between two sidebands. However, when an FP-FBG feature with a narrow notch is introduced to filter out one sideband, a phase modulation to intensity modulation (PM-IM) conversion is realized, and a microwave signal is generated at the output of the PD. Thus, in conjunction with the TLS and PM, the FP-FBG operates as a microwave photonic filter (MPF) to perform the frequency selection for the OEO. The oscillating microwave frequency corresponds to the difference between the frequency of the optical carrier and the frequency of the narrow notch, which is given by

$$f_M = f_c - f_{FP-FBG} \approx c \cdot \left(\frac{\lambda_{FP-FBG} - \lambda_c}{\lambda_c^2} \right) \tag{2}$$

where f_c and λ_c are the frequency and the wavelength of the optical carrier, f_{FP-FBG} and λ_{FP-FBG} are the frequency and the wavelength of the narrow notch of the FP-FBG respectively, and c is the velocity of light in vacuum.

As shown in Fig. 2(a), the sensing FP-FBG is fabricated by leaving a gap sandwiched between two identical FBGs aligned in a silica V-shape slot. The gap is filled with liquid under test. When the RI of liquid or surrounding temperature changes, the narrow notch of the FP-FBG will be shifted. Furtherly, the microwave frequency generated by the OEO would shift correspondingly. Now, a relationship will be theoretically analyzed between the optical distance of two cross sections and the center wavelength of the notch. For the Fabry-Perot interferometer, the wavelength of a resonance mode λ_R must satisfy

$$m\lambda_R = 2[n_s L_s + n_{eff}(2L_{eff} + L)] \tag{3}$$

where m is the resonance modal number of the Fabry-Perot interferometer, n_s is the RI of liquid, n_{eff} is the effective RI of the fiber core, L_s is the distance between two cross sections of the FBGs, L is the distance between two FBGs before they are cleaved and L_{eff} is the effective length owing to one FBG, which is given by [11]

$$L_{eff} = \frac{\lambda_{FBG}}{2\pi\overline{\delta n}} \tanh\left(\frac{\pi\overline{\delta n}}{\lambda_{FBG}} L_{FBG} \right) \tag{4}$$

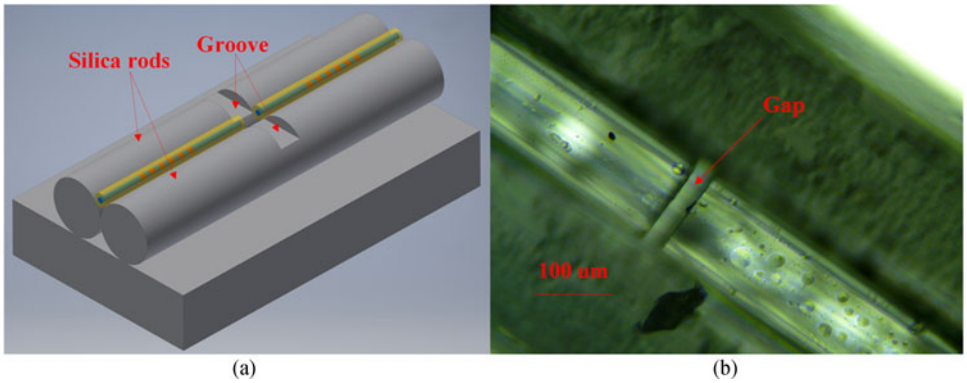

Fig. 2. (a) Schematic of the FP-FBG with a gap. (b) The microscopic image of the proposed FP-FBG structure.

where $\overline{\delta n}$ is the grating amplitude, λ_{FBG} is the center wavelength of FBG and L_{FBG} is the length of the FBG. From Eq. (3) and (4), the wavelength of the narrow notch of the FP-FBG is given by

$$\lambda_{FP-FBG} = \frac{2\left\{n_s L_s + n_{eff}\left[2\frac{\lambda_{FBG}}{2\pi\overline{\delta n}}\tanh\left(\frac{\pi\overline{\delta n}}{\lambda_{FBG}}L_{FBG}\right) + L\right]\right\}}{m} \tag{5}$$

where λ_{FP-FBG} is the wavelength of one resonance mode which is located in the filter range of the FBG by selecting appropriate modal number m in Eq. (5). For simplifying the relationship between the variation of the RI Δn_s and the wavelength shift of the notch of FP-FBG $\Delta\lambda_{FP-FBG}$, Eq. (3) is approximated by $m \approx \langle n_{eff}\frac{4L_{eff}+2L}{\lambda_{FBG}}\rangle (L_s << L_{eff})$ in small range variation of the RI, where $\langle x\rangle$ denotes to round x to the nearest integer. Through the approximation, the relationship is derived as

$$\Delta\lambda_{FP-FBG} = \frac{2\Delta n_s L_s}{\left\langle n_{eff}\left[\frac{2}{\pi\overline{\delta n}}\tanh\left(\frac{\pi\overline{\delta n}}{\lambda_{FBG}}L_{FBG}\right) + \frac{2L}{\lambda_{FBG}}\right]\right\rangle} \tag{6}$$

As shown in Eq. (6), the wavelength of the notch of FP-FBG will be linearly shifted to the longer wavelength with the increasing of the RI in small scale. The numerical simulation of the spectra of the FP-FBG with different RIs of liquid can also verify the relationship, as shown in Fig. 3(a). The effective RI of the fiber core is 1.4681, the length of FBG is 10 mm, the distance between two FBGs is 8 mm, the distance between two cross sections of the FBGs is 26 μm and the grating amplitude $\overline{\delta n}$ is 1.5×10^{-4}. Combining Eq. (2) and Eq. (6), the corresponding frequency change of the microwave signal is obtained by

$$\Delta f_M = -\frac{c}{{\lambda_c}^2} \cdot \frac{2\Delta n_s L_s}{\left\langle n_{eff}\left[\frac{2}{\pi\overline{\delta n}}\tanh\left(\frac{\pi\overline{\delta n}}{\lambda_{FBG}}L_{FBG}\right) + \frac{2L}{\lambda_{FBG}}\right]\right\rangle} \tag{7}$$

As can be seen the frequency change is also linearly proportional to the RI of liquid filled in the FP-FBG. As shown in Fig. 3, the lower sideband is filtered out by the notch of FP-FBG, and the wavelength change is mapped to the beating frequency between the upper sideband and the optical carrier.

As the ambient temperature changes, the effective RI of the fiber core changes due to the thermo-optic effect, which plays the dominant role with a thermo-optic coefficient p of $7.8 \times 10^{-6}/^{o}$C compared with a small thermal expansion coefficient $4.1 \times 10^{-7}/^{o}$C which can be ignored [12]. Because the little themo-optic coefficient causes the tiny change of the effective RI of the fiber core, m can remain constant. Thus, according to Eq. (5), the relationship between the wavelength shift

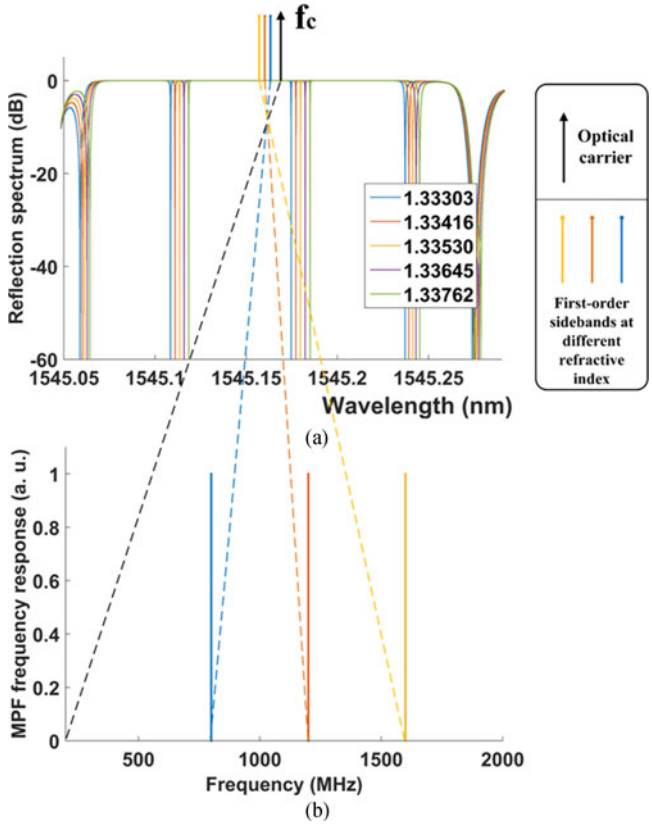

Fig. 3. (a) The numerical simulation of the reflection spectra of the FP-FBG with different RIs. (b) The principle of the FP-FBG-based OEO sensor.

of the notch of the FP-FBG and the variation of the surrounding temperature ΔT is derived by

$$\Delta\lambda_{FP-FBG} = \frac{2p\,\Delta T n_{eff}\left[\frac{\lambda_{FBG}}{\pi\overline{\delta n}}\tanh\left(\frac{\pi\overline{\delta n}}{\lambda_{FBG}}L_{FBG}\right)+L\right]}{\left\langle n_{eff}\left[\frac{2}{\pi\overline{\delta n}}\tanh\left(\frac{\pi\overline{\delta n}}{\lambda_{FBG}}L_{FBG}\right)+\frac{2L}{\lambda_{FBG}}\right]\right\rangle} \tag{8}$$

Combining Eq. (2) and Eq. (8), the corresponding frequency change of the microwave signal is obtained by

$$\Delta f_M = -\frac{c}{{\lambda_c}^2}\cdot\frac{2p\,\Delta T n_{eff}\left[\frac{\lambda_{FBG}}{\pi\overline{\delta n}}\tanh\left(\frac{\pi\overline{\delta n}}{\lambda_{FBG}}L_{FBG}\right)+L\right]}{\left\langle n_{eff}\left[\frac{2}{\pi\overline{\delta n}}\tanh\left(\frac{\pi\overline{\delta n}}{\lambda_{FBG}}L_{FBG}\right)+\frac{2L}{\lambda_{FBG}}\right]\right\rangle} \tag{9}$$

According to Eq. (8) and Eq. (9), the wavelength of the notch of the FP-FBG will be shifted linearly with the temperature, which is mapped to the frequency shift of microwave signal by the OEO correspondingly.

3. Experiment and Analysis

A proof-of-concept experiment based on the setup illustrated in Fig. 1 is demonstrated. The parameters of the major components in the experiment are given as follows: the center wavelength of light wave output is from the TLS (Agilent 8164A). The PM (EOSPACE) has a 3-dB bandwidth of 10 GHz and a half-wave voltage of 3 V. The gain and bandwidth of the EA (SHF 806E) are 26 dB and 38 GHz respectively. An ESA (Agilent N9010A) with a measuring range of 9 KHz $\sim$ 26.5 GHz is used to monitor the frequency spectrum. The special FP-FBG in the OEO loop is fabricated

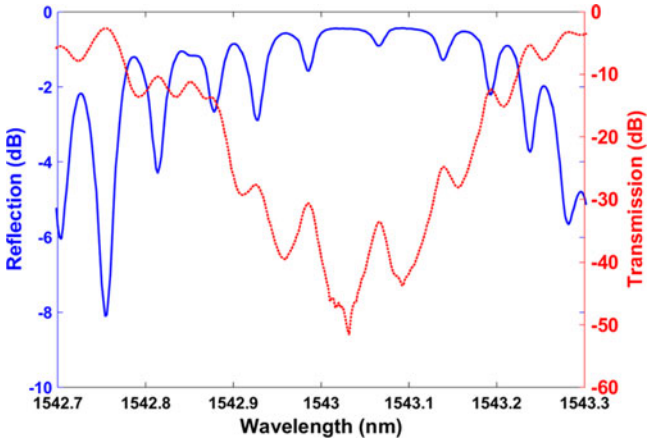

Fig. 4. The reflection and transmission spectra of the FP-FBG.

as follows: an ordinary FP-FBG consisted of two 10 mm length FBGs with 8 mm separation is written on a hydrogen-loaded fiber by using a phase mask with a period of 1068 nm exposed under a 248 nm KrF excimer laser ultraviolet light. Then the ordinary FP-FBG is cleaved in the middle position between the two FBGs. To align two FBGs, a V-shape slot is fabricated by a glass slide and two silica rods which have identical thermal expansion coefficients with optical fiber. Firstly, two silica rods with 300 μm diameter are held together in parallel and glued onto the glass slide with instant adhesive. Between the two rods, a V-shape slot is formed and used to fix two optical fibers with FBGs in the slot. Secondly, a groove is milled out along the direction perpendicular to the axis of rods. The depth of the groove is slightly more than 62.5 μm, which guarantees the air to be squeezed out from the groove after the liquid is filled. Finally, one FBG is fixed in the V-shape slot by the instant adhesive and another FBG is aligned to it. To guarantee the extremely narrow notch filter, an optical spectrum analyzer (OSA, ANDO AQ6317C) is used to monitor the transmission spectra during the fabrication of the FP-FBG. To constitute the gap cavity of FP-FBG, the fiber is aligned to the fixed fiber by adjusting the angle of depression and elevation, the angle of lateral swing and the distance between two fiber end faces in the V-shape slot under a microscope. Fig. 2(b) shows one microscopic image of the fabricated FP-FBG. Meanwhile, the gap needs to be at the same position as the groove. In this experiment, the distance between the two fiber cross sections is 26 μm. The reflection and transmission spectra of the FP-FBG are measured by the OSA with a wavelength resolution of 0.01 nm, as shown in Fig. 4. The loss of the FP-FBG is 1.73 dB. The center wavelength of the narrow notch is about 1543.066 nm, and the 3 dB bandwidth of the reflection spectrum is about 0.154 nm. However, due to the limited measuring resolution of the OSA, the details of the notch cannot be afforded by a zoomed-in view.

Adjusting the polarization by tuning the PC to minimize the polarization-dependent loss, the OEO starts to oscillate with the laser power of 5 mW. The center frequency of the microwave signal generated by the OEO is about 4.7 GHz, which is measured by the ESA. To study the stability of the proposed OEO, the electrical spectra of the signal with a frequency span of 10 GHz are repeatedly measured 11 times in half an hour with a time interval of 3 mins, as shown in Fig. 5(a). There are no obvious frequency fluctuations in 30 mins. Furtherly, the stability of the OEO with span of 100 MHz are measured 11 times in 10 minutes with a time interval of 1 min, as shown in Fig. 5(c). The measured frequency in 10 mins is below 30 KHz and the power fluctuations in 10 mins is below 0.56 dB, respectively, as shown in Fig. 5(d). As shown in Fig. 5(b), the FSR of the OEO is about 10.4 MHz and the side-mode suppression ratio is about 48.3 dB. It should be noted that the adjacent oscillating modes cannot be filtered out by the proposed MPF and suppressed completely owing to the large bandwidth of the notch of FP-FBG, but a single mode oscillating operation with no mode hopping is guaranteed during the experimental process.

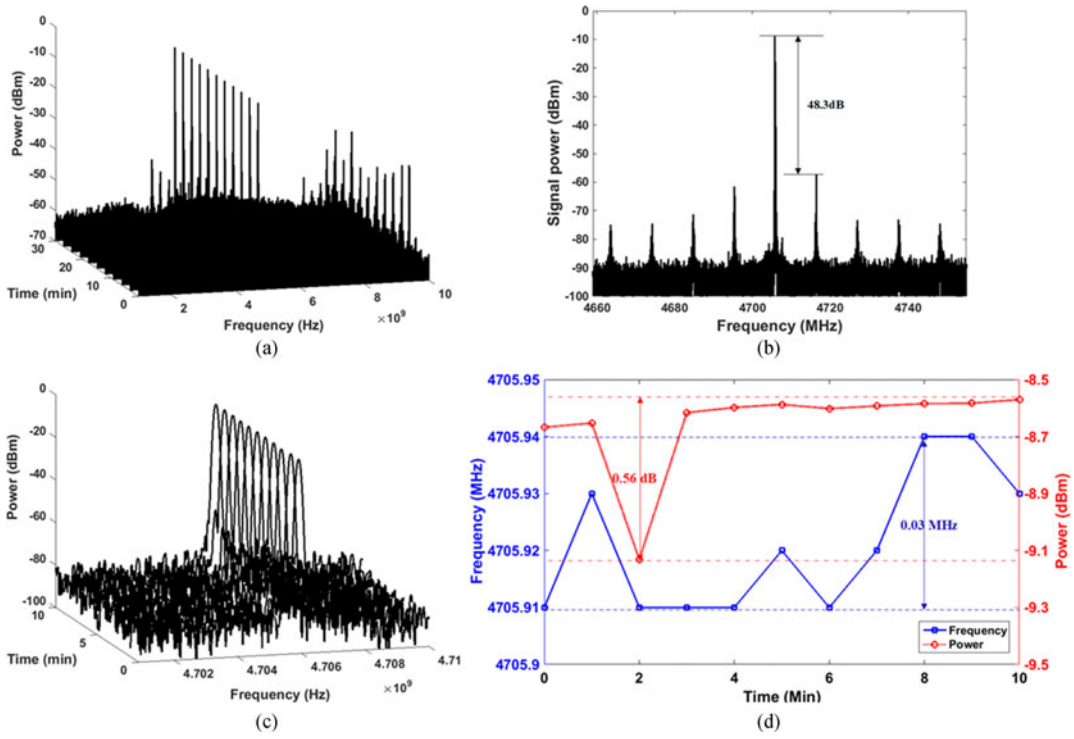

Fig. 5. (a) The superimposed electrical spectra of the generated signal at a 3-min interval over 30-min period (Span = 10 GHz, resolution bandwidth (RBW) = 3 MHz). (b) A certain measured electrical spectrum of the signal (Span = 100 MHz, RBW = 10 kHz). (c) Zoom-in view of the superimposed electrical spectra at a time interval of 1 min within 10 min (Span = 10 MHz, RBW = 91 kHz). (d) The frequency and power fluctuations in 10 min.

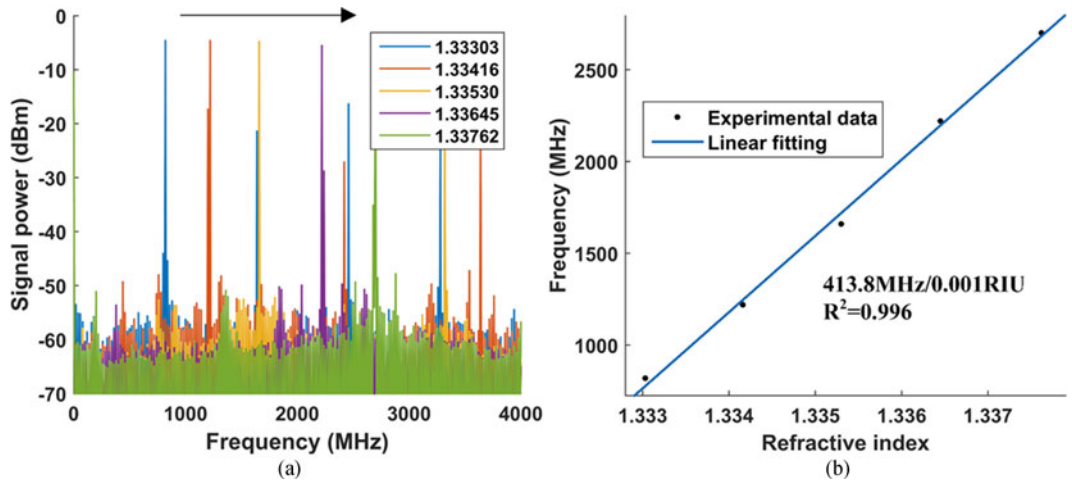

Fig. 6. (a) The electrical spectra of the generated microwave signal at the output of the PD with an increasing RI of liquid. (b) The relationship between the RI and the microwave signal frequency.

Different RI liquid is filled into the gap. Fig. 6(a) shows the electrical spectra of the generated microwave signal at the output of the PD under different RIs. By increasing the RI of liquid applied to the gap, the signal frequency is shifted linearly toward a higher frequency. Fig. 6(b) shows a linear fitting between the signal frequency and the RI. The RI sensitivity is about 413.8 MHz/0.001RIU with a correlation coefficient (R^2) of 0.996.

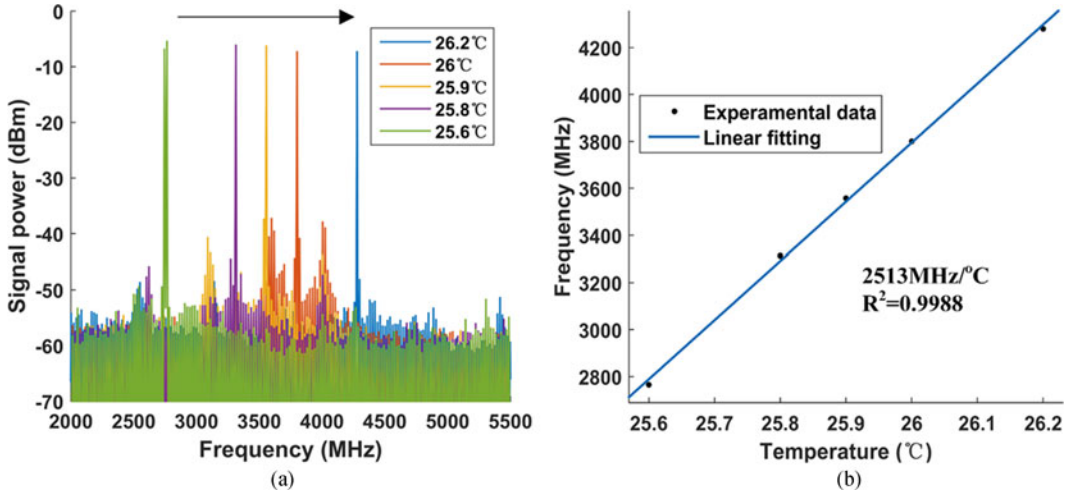

Fig. 7. (a) The electrical spectra of the generated microwave signal at the output of the PD with an increasing temperature. (b) The relationship between the temperature and the microwave signal frequency.

Then the measurement of the temperature by the OEO sensor is investigated. Fig. 7(a) shows the electrical spectra of the generated microwave signal at the output of the PD under different temperatures. By increasing the temperature of the external environment, the signal frequency is shifted linearly toward a higher frequency. A linear fitting is done between the signal frequency and the temperature. The temperature sensitivity as high as 2516 MHz/°C with an R^2 of 0.9988 is achieved.

4. Conclusion

We have proposed and experimentally demonstrated a scheme to interrogate the RI of liquid and temperature by using an FP-FBG based OEO. To implement the interrogation of the RI, a gap between fiber cross sections of two FBGs was fabricated in a silica V-shape slot to form an FP-FBG as sensing head, which also operated as a frequency selection component of OEO. The frequency shift of the microwave signal as a function of the RI of liquid and surrounding temperature of FP-FBG has been theoretically analyzed. By monitoring the signal frequency, the RI and the temperature sensing have been investigated experimentally, which was in accord with the theoretical analysis. An ultra-high RI sensitivity of 413.8 MHz/0.001RIU and temperature sensitivity of 2516 MHz/°C have been obtained.

References

[1] C. R. Liao, T. Y. Hu, and D. N. Wang, "Optical fiber Fabry-Perot interferometer cavity fabricated by femtosecond laser micromachining and fusion splicing for refractive index sensing," *Opt. Exp.*, vol. 20, no. 20, pp. 22813–22818, Sep. 2012.
[2] T. Hu, Y. Zhao, and A. Song, "Fiber optic SPR sensor for refractive index and temperature measurement based on MMF-FBG-MMF structure," *Sens. Actuators B Chem.*, vol. 237, pp. 521–525, 2016.
[3] Z. L. Xu *et al.*, "Highly sensitive refractive index sensor based on cascaded microfiber knots with Vernier effect," *Opt. Exp.*, vol. 23, no. 5, pp. 6662–6672, Mar. 2015.
[4] S. Zhu, F. F. Pang, S. J. Huang, F. Zou, Y. H. Dong, and T. Y. Wang, "High sensitivity refractive index sensor based on adiabatic tapered optical fiber deposited with nanofilm by ALD," *Opt. Exp.*, vol. 23, no. 11, pp. 13880–13888, Jun. 2013.
[5] J. Yao, "Optoelectronic oscillator for high speed and high resolution optical sensing," *J. Lightw. Technol.*, vol. 35, no. 16, pp. 3489–3497, Jun. 2017.
[6] O. Xu, J. J. Zhang, H. Deng, and J. P. Yao, "Dual-frequency optoelectronic oscillator for thermal-insensitive interrogation of a FBG strain sensor," *IEEE Photon. Technol. Lett.*, vol. 29, no. 4, pp. 357–360, Feb. 2017.
[7] F. Q. Kong, B. Romeira, J. J. Zhang, W. Z. Li, and J. P. Yao, "A dual-wavelength fiber ring laser incorporating an injection-coupled optoelectronic oscillator and its application to transverse load sensing," *J. Lightw. Technol.*, vol. 20, no. 9, pp. 1784–1793, May 2014.

[8] B Yin, M. G. Wang, S. H. Wu, Y. Tang, S. C. Feng, and H. W. Zhang, "High sensitivity axial strain and temperature sensor based on dual-frequency optoelectronic oscillator using PMFBG Fabry-Perot filter," *Opt. Exp.*, vol. 25, no. 13, pp. 14106–14113, Jun. 2017.
[9] L. D. Nguyen, K. Nakatani, and B. Journet, "Refractive index measurement by using an optoelectronic oscillator," *IEEE. Photon. Technol. Lett.*, vol. 22, no. 12, pp. 857–859, Jun. 2010.
[10] W. Z. Li and J. P. Yao, "A wideband frequency tunable optoelectronic oscillator incorporating a tunable microwave photonic filter based on phase-modulation to intensity-modulation conversion using a phase-shifted fiber Bragg grating," *IEEE Trans. Microw. Theory Techn.*, vol. 60, no. 6, pp. 1735–1742, Jun. 2012.
[11] Y. O. Barmenkov, D. Zalvidea, S. Torres-Peiró, J. L. Cruz, and M. V. Andrés, "Effective length of short Fabry-Perot cavity formed by uniform fiber Bragg gratings," *Opt. Exp.*, vol. 14, no. 14, pp. 6394–6399, Jul. 2006.
[12] C. R. Liao, H. F. Chen, and D. N. Wang, "Ultracompact optical fiber sensor for refractive index and high-temperature measurement," *J. Lightw. Technol.*, vol. 32, no. 14, pp. 2531–2535, Jul. 2014.